PNL-6630
UC-85

Comparison of HYDRA-II Predictions to Temperature Data from Consolidated and Unconsolidated Model Spent Fuel Assemblies

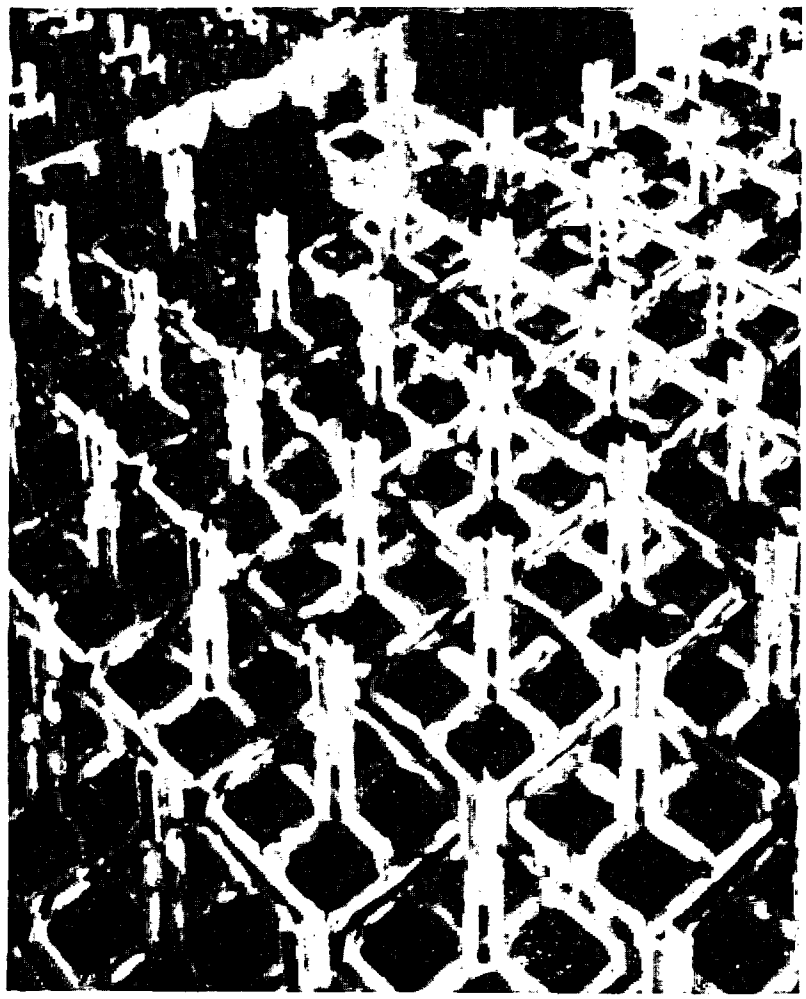

September 1988

Prepared for the U.S. Department of Energy
under Contract DE-AC06-76RLO 1830

Pacific Northwest Laboratory
Operated for the U.S. Department of Energy
by Battelle Memorial Institute

PNL-6630

DISCLAIMER

PACIFIC NORTHWEST LABORATORY
operated by
BATTELLE MEMORIAL INSTITUTE
for the
UNITED STATES DEPARTMENT OF ENERGY
under Contract DE-AC06-76RLO 1830

Printed in the United States of America
Available from
National Technical Information Service
United States Department of Commerce
5285 Port Royal Road
Springfield, Virginia 22161

NTIS Price Codes
Microfiche A01

Printed Copy

Pages	Price Codes
001-025	A02
026-050	A03
051-075	A04
076-100	A05
101-125	A06
126-150	A07
151-175	A08
176-200	A09
201-225	A10
226-250	A11
251-275	A12
276-300	A13

PNL-6630
UC-85

COMPARISON OF HYDRA-II PREDICTIONS TO TEMPERATURE DATA FROM CONSOLIDATED AND UNCONSOLIDATED MODEL SPENT FUEL ASSEMBLIES

R. A. McCann

September 1988

Prepared for
the U.S. Department of Energy
under Contract DE-AC06-76RLO 1830

Pacific Northwest Laboratory
Richland, Washington 99352

ABSTRACT

Using the HYDRA-II computer code, Pacific Northwest Laboratory (PNL) researchers analyzed the thermal performance of two model spent fuel assemblies. The numerical simulations were based on information from offsite laboratory tests conducted previously on an unconsolidated and a consolidated rod assembly. The objectives of the PNL effort were to examine the thermal characteristics of the consolidated rod assembly and to validate the predictive capability of the HYDRA-II code for application to such analyses. When compared to the physical test data, the predictions generated by HYDRA-II were in excellent agreement for all temperature comparisons. These analyses provided further validation of HYDRA-II's capability to accurately predict thermal performance of spent fuel storage system components. Results obtained for the consolidated rod assembly lend strong support to the value of further investigations of this option for dry storage of spent fuel.

SUMMARY

Pacific Northwest Laboratory (PNL) researchers analyzed the heat transfer performance of two model spent fuel assemblies, using the HYDRA-II computer code developed earlier at PNL. The analyses extended previous research on systems for dry storage of spent fuel being conducted for the U.S. Department of Energy by PNL's Commercial Spent Fuel Management Program. The objectives of the analyses were to examine thermal characteristics of consolidated fuel rod assemblies and to validate the predictive capabilities of the HYDRA-II code for use in consolidated assembly evaluations.

The HYDRA-II simulations were based on data from previously conducted laboratory tests of two model spent fuel assemblies. Both assemblies (one unconsolidated, the other consolidated) contained electrically heated rods simulating fuel from 8 x 8-rod boiling water reactor (BWR) assemblies. The unconsolidated assembly comprised 64 rods, 63 of which were heated, arranged on a square pitch to simulate a typical BWR assembly. This assembly was contained in a stainless steel tube simulating a boral fuel tube from a dry storage cask. The consolidated assembly consisted of 126 rods (the equivalent of two 8 x 8 BWR assemblies with 63 active rods each), arranged on a triangular pitch. The rods were confined within a canister that fit inside the stainless steel tube previously used in the unconsolidated tests. Via strategically placed thermocouples, temperatures were measured in these test sections under varying conditions of fill gas (helium and air), equivalent BWR assembly power level (400 W and 800 W), and rod-to-rod gap (0.0 in. and 0.01 in).

Information on the test section configurations, material properties, and boundary conditions from the physical tests was used by PNL to construct the input file for the HYDRA-II simulations. The thermal performance predictions generated by HYDRA-II were then compared to the physical test results.

Upon comparison, the HYDRA-II-computed temperatures were found to be in excellent agreement with the temperatures measured during the physical tests. This overall result provides a basis for establishing an acceptable and

verifiable level of confidence in the HYDRA-II code's predictive capabilities. Other significant conclusions drawn from this analysis effort include the following:

- The thermal conductivity of the backfill gas has a significant effect on rod temperatures. The peak rod temperatures in helium were approximately 0.4 times those measured in air. This relationship held steady for rod-to-rod gaps of both 0.0 and 0.01 in.
- The increase in temperature of the rods above the external fuel tube is approximately proportional to the power dissipated in the assembly. The temperature difference would be exactly proportional to power in the absence of nonlinearities such as temperature-dependent thermal conductivities, radiation, and natural convection (if present).
- The effect on temperature of varying rod-to-rod gaps in the consolidated assembly was predictable but relatively small. When the rod-to-rod gap was increased from 0.0 to 0.01 in., the difference between peak rod temperature and fuel tube temperature increased by about 20%, regardless of fill gas type.
- An assembly in contact with its fuel tube or support structure may have a reduced peak temperature relative to that of a symmetrically located assembly. The reduction in temperature is relatively small, however, compared to the temperature difference between the assembly centerline and fuel tube.
- The effectiveness of consolidation on heat dissipation was substantial. The effective thermal conductivity of a consolidated rod assembly was approximately twice that of an unconsolidated assembly. A consolidated rod assembly that generates twice as much heat as an unconsolidated assembly will therefore have nearly the same temperature rise above the fuel tube temperature. However, the absolute temperatures of the fuel rods contained in storage systems are dependent also upon heat transfer paths from the fuel tubes to the exterior environment.

- The HYDRA-II computer code's capability to predict consolidated rod assembly thermal behavior is excellent. The mean deviation between HYDRA-II predictions and physical test data for all temperature comparisons was ±0.03°C. The standard deviation of ±2.5°C is comparable to the experimental uncertainty reported for the physical tests. The results for the unconsolidated rod assembly were also excellent.

Based on this analysis effort, two recommendations are offered:

- Assessments of the rod consolidation alternative for dry storage of spent fuel should continue. No significant heat transfer deficiencies were noted in this study. In addition, the reduced volume achieved by consolidating spent fuel rods is a positive feature.
- The HYDRA-II computer code should continue to be considered for use to obtain best-estimate predictions of thermal performance of spent fuel storage systems containing either consolidated or unconsolidated assemblies.

ACKNOWLEDGMENTS

Appreciation is extended to the U.S. Department of Energy for sponsoring this work. Appreciation is also extended to G. H. Beeman and J. M. Creer of the Commercial Spent Fuel Management Program at Pacific Northwest Laboratory. Project management was provided by C. L. Wheeler and M. A. McKinnon. A. J. Currie provided technical editing support. Text processing was done by J. L. Moore and R. M. Moreno under the supervision of S. E. Yost.

CONTENTS

FIGURES

TABLES

COMPARISON OF HYDRA-II PREDICTIONS TO TEMPERATURE DATA FROM CONSOLIDATED AND UNCONSOLIDATED MODEL SPENT FUEL ASSEMBLIES

1.0 INTRODUCTION

Implementation of spent fuel dry storage systems is required in the late 1980s because several at-reactor storage basins will attain maximum capacity, according to U.S. Department of Energy (DOE) sources (1986). The Nuclear Waste Policy Act of 1982 (NWPA) assigns DOE the responsibility for assisting utilities with their spent fuel storage problems. The NWPA specifies further that DOE shall provide generic research and development of alternative spent fuel storage systems to assist utilities in their licensing activities.

The Commercial Spent Fuel Management (CSFM) Program at the Pacific Northwest Laboratory (PNL)[a] currently supports DOE efforts to meet its NWPA mandate. Through the CSFM Program, various methods for increasing storage capacity are being evaluated. Among the alternatives being considered is consolidation, in which a spent fuel assembly is disassembled and the individual rods are repackaged in a closely-packed array. Two spent fuel assemblies can be consolidated into a space approximately equal to that of one original assembly. The repackaged consolidated spent fuel may then be placed in a dry storage system (e.g., metal cask, concrete silo, or vault).

Regardless of type, all spent fuel dry storage systems must dissipate heat while maintaining the temperature of the stored fuel rods below established limits. A storage system's thermal performance can be assessed by a comprehensive testing program. However, such testing programs are typically time-consuming and expensive. Analysis tools (e.g., computer codes), while not intended to entirely supplant tests, can help reduce those costs.

(a) Operated by Battelle Memorial Institute for the U.S. Department of Energy under Contract DE-AC06-76RLO 1830.

Appropriately qualified computer codes can provide predictions of thermal performance as a function of system design and operating conditions. Moreover, when tests are to be performed, computer codes can help select test conditions, spent fuel decay heat generation rates, and instrumentation placements, as well as aid in interpreting test data. The qualification of a code for a given application generally involves comparing the code predictions with results of relevant tests. The credibility of a code is proportionately increased by the number of favorable comparisons that can be provided.

This report documents heat transfer analyses of two electrically heated model spent fuel assemblies. One model assembly represented a typical unconsolidated boiling water reactor (BWR) fuel assembly; the other represented a consolidation of two BWR assemblies into a closely-packed hexagonal array of rods. Pacific Northwest Laboratory researchers used the HYDRA-II computer code to numerically simulate the assemblies' thermal performance. The objectives of this effort were to determine the thermal characteristics of the consolidated rod assembly and to validate the predictive capabilities of the HYDRA-II code for use in future studies of the consolidated fuel alternative. HYDRA-II predictions were compared previously to two sets of unconsolidated assembly data (McCann 1986) and two sets of multiassembly storage cask data (Wiles et al. 1986; Creer et al. 1986).

The conclusions and recommendations drawn from the results of these analyses are presented in Section 2.0. A brief overview of the HYDRA-II code is presented in Section 3.0. The experimental test sections for the unconsolidated and consolidated rod assemblies are described in Section 4.0. Modeling uncertainties are discussed in Section 5.0. In Section 6.0, the computational methodology is documented, followed by the comparisons of HYDRA-II predictions to experimental data for the two model assemblies.

2.0 CONCLUSIONS AND RECOMMENDATIONS

The HYDRA-II computer code was used to predict the thermal performance of two electrically heated model spent fuel assemblies. One rod assembly represented a typical unconsolidated BWR spent fuel assembly; the other represented a two-to-one consolidation of rods in a hexagonal array. Comparison of the computed temperatures with those obtained from experimental tests provides a basis for establishing an acceptable and verifiable level of confidence in the code's predictive capabilities. Important conclusions and recommendations established from the work described in this report are presented in this section.

2.1 CONCLUSIONS

Six principal conclusions were drawn from the work described in this report:

- The thermal conductivity of the backfill gas has a significant effect on rod temperatures. Helium and air backfill gases were used in the consolidated test section. The thermal conductivity of helium is approximately five times higher than that of air at the test temperatures. The peak rod temperatures in helium were approximately 0.4 times those in air. This relationship held for rod-to-rod gaps of 0.0 in. and 0.01 in.
- The temperature differences between rods and the external fuel tube were, in all cases, approximately proportional to the power dissipated in the assembly. The temperature differences would be exactly proportional to power in the absence of nonlinearities such as temperature-dependent thermal conductivities, radiation, and natural convection (if present).
- The temperature effect of varying rod-to-rod gaps in the consolidated rod assembly is predictable but relatively small. As the rod-to-rod gap was increased from 0.0 in. to 0.01 in., the

difference between peak rod temperature and fuel tube temperature increased by approximately 20%. This was true for both helium and air in the simulated test section.

- An assembly that is in contact with its fuel tube or support structure may have a reduced peak temperature relative to a symmetrically located assembly. The reduction in temperature is relatively small, however, compared to the temperature difference between assembly centerline and fuel tube.
- The effectiveness of consolidation is substantial. For illustration, a comparison may be made between the unconsolidated test section with air backfill to the consolidated test section with air backfill and a rod-to-rod gap of 0.01 in. This comparison shows that, for equal power, the difference between peak rod temperature and fuel tube temperature is approximately 1.4 times higher for the unconsolidated rod assembly. If both test sections had equal end heat losses (as would be the case for full-length rods), it is estimated that the temperature rise for the unconsolidated rods would be about twice that of the consolidated rods. Stated another way, an assembly consolidated two-to-one would have about the same peak temperature (relative to the fuel tube) as an unconsolidated assembly, provided that the heat generation rate per rod is the same. However, the absolute temperature of fuel rods contained within a spent fuel storage system (i.e., cask) also depends on the hydrothermal performance of the system, from the fuel tubes to the exterior environment, for the total amount of heat generated.
- The HYDRA-II computer code's predictive capability for consolidated rod assemblies was excellent. The mean deviation between predictions and data for all temperature comparisons was ±0.03°C, with a standard deviation of ±2.5°C. This standard deviation is comparable to the reported experimental uncertainty in this data. The results for the unconsolidated rod assembly were also excellent; however, the good agreement between predictions and data was

largely fortuitous. Unavailability of test documentation renders the unconsolidated assembly data set unsuitable for code validation.

2.2 RECOMMENDATIONS

Recommendations based on the results of, and conclusions drawn from, this work are:

- The rod consolidation alternative for spent fuel dry storage should continue to be investigated. No significant heat transfer deficiencies are apparent from the results of this study. The reduced volume acquired per assembly, by itself, is potentially attractive in an appropriately designed spent fuel storage system.
- The HYDRA-II computer code should continue to be considered for use to obtain best-estimate predictions of the thermal performance of spent fuel storage systems containing either consolidated or unconsolidated spent fuel assemblies.

3.0 HYDRA-II COMPUTER CODE CAPABILITIES

This section provides an overview of the current capabilities of HYDRA-II that are of special interest to spent fuel storage system analysis. HYDRA-II is a fully three-dimensional hydrothermal computer code that solves the equations of fluid motion, continuity, and heat transfer by finite-difference techniques. HYDRA-II is constructed with reasonable generality and therefore has considerable applicability beyond storage system applications.

HYDRA-II has been assessed extensively using applications ranging from model problems with known analytic solutions to full-scale spent fuel storage casks with experimental data. Results of these previous assessments are summarized in McCann and Lowery (1987). The analyses of unconsolidated and consolidated assemblies reported here continue the series of applications intended to broaden the verifiable level of confidence in the code's predictive capabilities.

The time-dependent conservation equations of momentum and mass for compressible fluids are used as the basis for calculating single-phase flow fields. The time-dependent conservation equation of energy with convection and heat sources is the basis for calculating the temperature field. These conservation equations are as follows:

Momentum

$$\frac{\partial}{\partial t}(\vec{m}) = \rho\vec{g} - \nabla p - D\vec{m} + \nabla\cdot(\mu\nabla\vec{v}) - \nabla\cdot(\vec{v}\vec{m}) \qquad (3.1)$$

where t = time,
$\vec{m}$ = mass flux
ρ = density
$\vec{g}$ = gravitational vector
p = pressure
D = Darcy and orifice drag
μ = viscosity
$\vec{v}$ = velocity.

Mass

$$\frac{\partial}{\partial t}(\rho) = -\nabla\cdot(\vec{m}) \tag{3.2}$$

Energy

$$\frac{\partial}{\partial t}(\rho C_p T) = \nabla\cdot(\lambda\nabla T) - \nabla\cdot(C_p\vec{m}T) + \dot{q} \tag{3.3}$$

where C_p = specific heat
T = temperature
λ = thermal conductivity.

The source term, $\dot{q}$, in Equation (3.3) represents heat generation and thermal radiation transport. The latter is given by an expression of the form

$$\dot{q}_{rad\ i\to j} = H_{ij}\,(T_i^4 - T_j^4) \tag{3.4}$$

where H_{ij} is an exchange factor based on geometry and emittances. A thermodynamic state relationship of the form

$$\rho = f(p,T) \tag{3.5}$$

is required, as are other relationships needed to define temperature-dependent material properties.

The conservation equations are converted to finite-difference equations using the locally one-dimensional philosophy embodied in Spaulding's Hybrid scheme [see, for example, Patankar (1980)]. Both the energy equation and the three linear momentum equations are solved using an alternating-direction algorithm described by Douglas and Gunn (1964). The momentum equations are linked with the conservation of mass equation in a manner consistent with the spirit of the CTS SIMPLE algorithm described by Raithby and Schneider (1979, 1980). The numerics incorporated in HYDRA-II are described in detail in McCann (1987).

HYDRA-II uses a cartesian coordinate system for the computational mesh in the interior of casks. A cylindrical coordinate system is available for convenience in calculating the temperature field in an exterior cask body. When both coordinate systems are invoked to model a single application, the code will automatically align the two systems and enforce conservation of energy at their interface.

HYDRA-II is designed to provide a user-oriented input interface that eliminates the need for internal code changes. Any application for which the code is an appropriate choice can be completely described through the construction of an input file. The user may optionally request a formatted echo of the input file to confirm that the intended parameters are actually those used by the code. A selectable commentary monitoring the progress of the code toward a steady-state solution is available, as is a summary of energy balances. Finally, a tape may be written at the conclusion of a run, in the event that the user might wish to restart the solution from its most recent point. McCann, Lowery, and Lessor (1987) contains code flow charts, discusses the code structure, provides detailed instructions for preparing an input file, and illustrates the operation of the code by means of a model problem. The modeling capabilities available in HYDRA-II are summarized in Table 3.1.

TABLE 3.1. HYDRA-II Modeling Capabilities

Geometry and Numerics	• fully three-dimensional • variable grid spacing in both cartesian and cylindrical grids • several multi-grid schemes available to speed convergence of the momentum and energy solutions • several iterative schemes for use, alone or in combination, in obtaining solution for the fluid pressure field • "time" advance to steady state
Fluid Solution	• finite-difference on a cartesian grid • modeling a closed system • compressible, ideal gas • orifice- and Darcy-flow models • user-specified, orthotropic fluid permeabilities and subgrid scale obstructions • user-specified, temperature-dependent viscosity • fixed system-pressure or total-mass operation conditions
Thermal Solution	• finite-difference on a cartesian grid and, if desired, an enveloping cylindrical grid • modeling an open system • conduction, convection, and radiation heat transfer modes; correlation for natural convection heat transfer to the environment • user-specified, temperature-dependent and orthotropic conductivity • user-specified, spatially-dependent energy-source terms • several models for radiation heat transfer
Program and Input/ Output Control	• variably-dimensioned arrays (required core size specified by the user through PARAMETER statements) • restart and post-processing dumps • echoed input • user-specified convergence history monitoring

4.0 LABORATORY TEST DESCRIPTION

To assess the HYDRA-II code's validity for use in characterizing the thermal performance of consolidated spent fuel assemblies, PNL researchers used information from tests conducted previously by Ridihalgh, Eggers & Associates (REA) and Eggers Ridihalgh Partners, Inc. The test conditions and resulting measurements reported in Eggers (1985a, 1985b) provided the respective bases for the HYDRA-II input file created by PNL to generate predictions and the measure against which to compare those HYDRA-generated predictions. Because of their importance to the PNL effort, details of these previous tests are provided in this section.

4.1 UNCONSOLIDATED ASSEMBLY

The 24-in.-long unconsolidated assembly test section comprised 64 rods oriented horizontally on a square pitch, simulating a typical 8 x 8 BWR spent fuel assembly. Sixty-three of the rods were electrically heated to simulate the fuel. The overall assembly was installed in a stainless steel tube to represent a boral fuel tube of an REA 2023 dry storage cask.

A cross section of the geometry of the unconsolidated assembly is shown in Figure 4.1, with relevant dimensions marked in inches. The dimensions closely approximate the geometry of an 8 x 8 BWR fuel assembly, with 0.500-in.-diameter electrically heated rods and a pitch-to-diameter ratio of 1.3.

The electrically heated rods were tubes of black-anodized aluminum, filled with an insulating material. A heater wire centered in the tube generated an axially uniform power profile along the length. The anodized aluminum surface was reported to have an emittance ranging from 0.8 to 0.9, simulating the expected emittance of Zircaloy™ fuel rods after prolonged irradiation and pool storage. The emittance of the stainless steel fuel tube

™ A zirconium alloy manufactured by Westinghouse Electric Corporation, Specialty Metals Division, Blairsville, Pennsylvania.

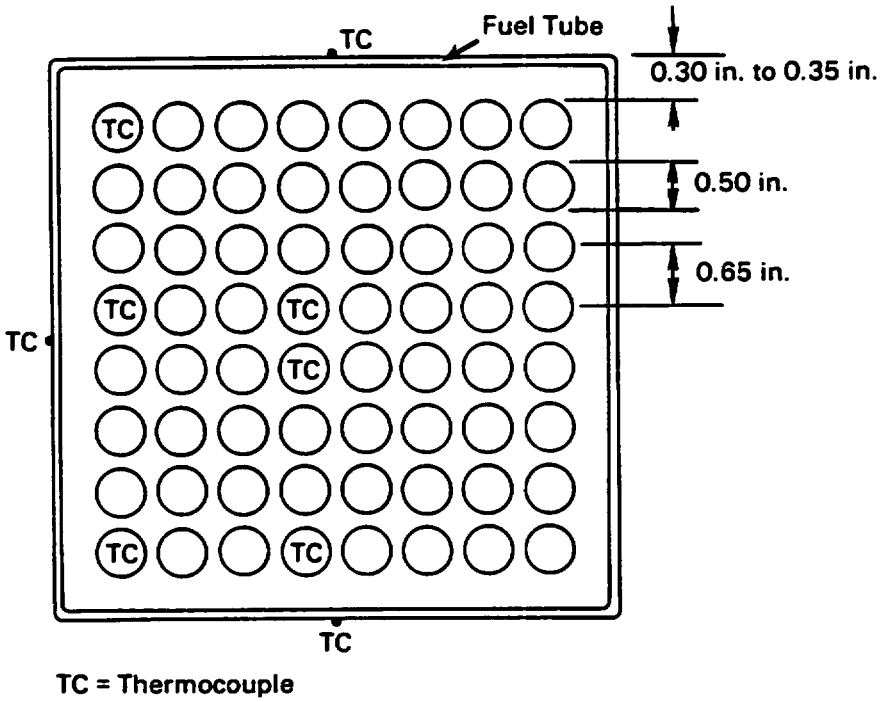

FIGURE 4.1. Unconsolidated Assembly Test Section

containing the assembly was assumed to be in the range of 0.2 to 0.3. The reported emittance ranges were based on vendor-supplied data or published values.

Figure 4.1 also indicates the radial locations of the thermocouples with which the measurements were taken. Three of the four sides of the fuel tube were instrumented, as were six of the heated rods. The thermocouples on the fuel tube were brazed to the outer surface of the plates, and those on the rods were inserted in holes drilled in the aluminum. The aluminum was pinched around the thermocouple wires to ensure good mechanical and thermal contact. Thermocouples were located at the radial positions indicated in Figure 4.1 at three axial levels along the assembly heated length. Plane A was 2 in. from one end of the assembly, Plane B was the midplane of the assembly, and Plane C was 2 in. from the other end of the assembly, as shown in Figure 4.2.

The unconsolidated test section was operated at two power levels equivalent to decay heat rates of 400 W and 800 W for an actual BWR spent fuel

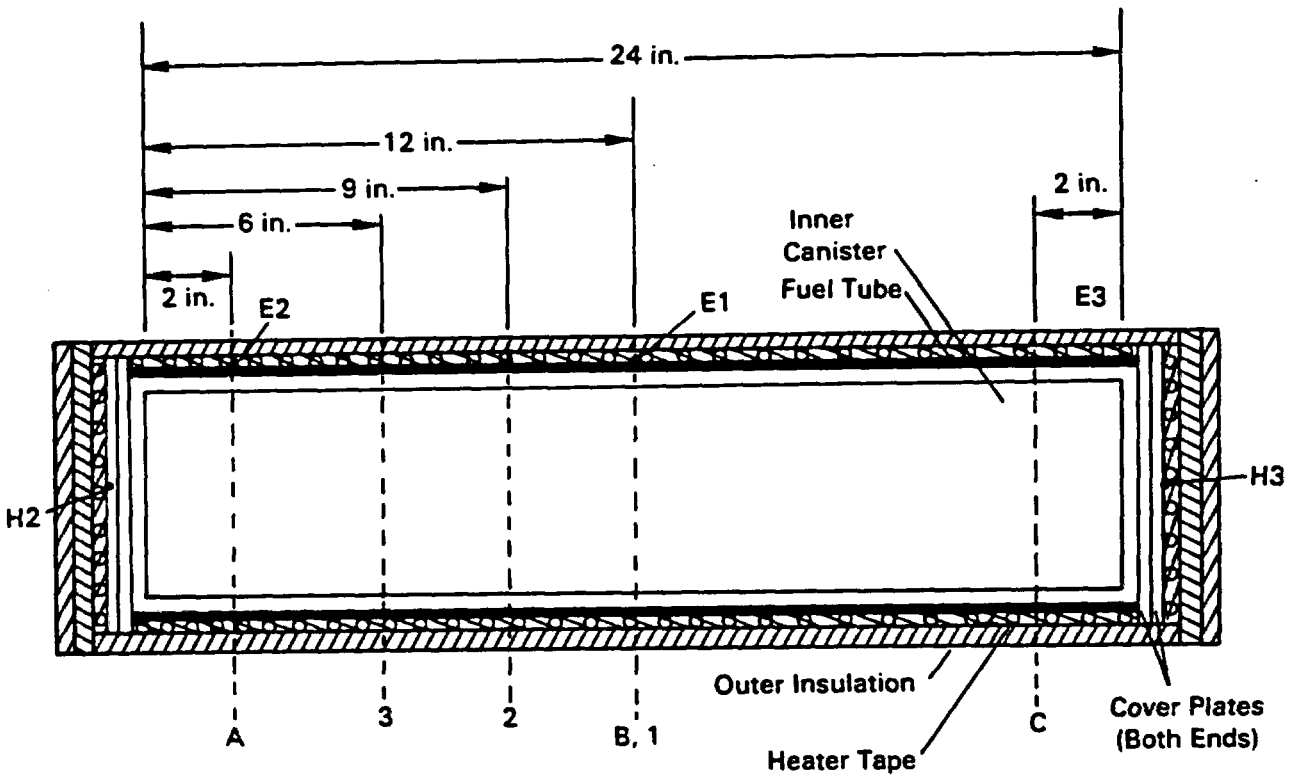

FIGURE 4.2. Axial Locations of Thermocouple Measurement Planes in the Consolidated and Unconsolidated Test Sections

assembly. The 400-W decay heat rate is approximately that generated in a BWR spent fuel assembly with a burnup of 33,000 MWd/MTU and a cooling time of 5 years. Neglecting the effect of axial peaking encountered in an actual BWR fuel assembly, this translated into an operating power of 400/6 W, or 66.7 W, for the 24-in.-long test section. The desired boundary temperature was imposed on the test section by means of an electric heater tape wrapped around the outer surface of the fuel tube.

Six tests were conducted on the unconsolidated assembly test section, as summarized in Table 4.1. Four of the tests were conducted with air at atmospheric pressure; the other two were conducted in vacuum. The pressure for the vacuum tests was reported as less than 10^{-2} mm Hg. A pressure sufficiently low to permit the mean free path of the gas to exceed any significant dimension was not achieved. This is supported by test data (Eggers 1985b). The test matrix was thus essentially one with two power levels and fuel tube temperatures that ranged from 156°C to 205°C.

TABLE 4.1. Unconsolidated Assembly Test Matrix

Test	Internal Atmosphere[a]	Equivalent Decay Heat Level Per Unconsolidated Assembly, Watts[b]	Rod-to-Rod Gap, Inches[c]	Rod-to-Wall Gap, Inches[d]	Emittance[e]	
					Fuel Rods	Inner Canister Surface
U1	Air	400	0.15	0.30 to 0.35	0.8 to 0.9	0.2 to 0.3
U2	Air	400	0.15	0.30 to 0.35	0.8 to 0.9	0.2 to 0.3
U3	Air	800	0.15	0.30 to 0.35	0.8 to 0.9	0.2 to 0.3
U4	Vacuum[f] (air)	400	0.15	0.30 to 0.35	0.8 to 0.9	0.2 to 0.3
U5	Vacuum[f] (air)	800	0.15	0.30 to 0.35	0.8 to 0.9	0.2 to 0.3
U6	Air	400	0.15	0.30 to 0.35	0.8 to 0.9	0.2 to 0.3

(a) Atmosphere at atmospheric presure (~760 mm Hg) unless otherwise noted.
(b) Assumes constant decay heat generation rate over active length of BWR fuel assembly; nominal value.
(c) Rod diameter is 0.500 ±0.001 in.; actual rod-to-rod gap dimension has a tolerance of ±0.005 in.
(d) This gap is uniform on all four sides with tolerance of ±0.010 in.
(e) Emittance ranges based on vendor-supplied data or published values.
(f) $<10^{-2}$ mm Hg or $<10^{-2}$ Torr.

4.2 CONSOLIDATED ASSEMBLY

The consolidated assembly consisted of 126 rods (equal to two 8 x 8 assemblies with 63 active rods each), arranged on a triangular pitch. The rods were confined within a canister that fit inside the same stainless steel tube used to contain the unconsolidated assembly. The test section was 24 in. long overall.

A cross section of the geometry of the consolidated assembly is shown in Figure 4.3. The rods were of 304 stainless steel tubing (unlike those in the unconsolidated assembly, which were anodized aluminum tubing), with a nominal outside diameter of 0.500 in. and a 0.035-in.-thick wall. The tubes were

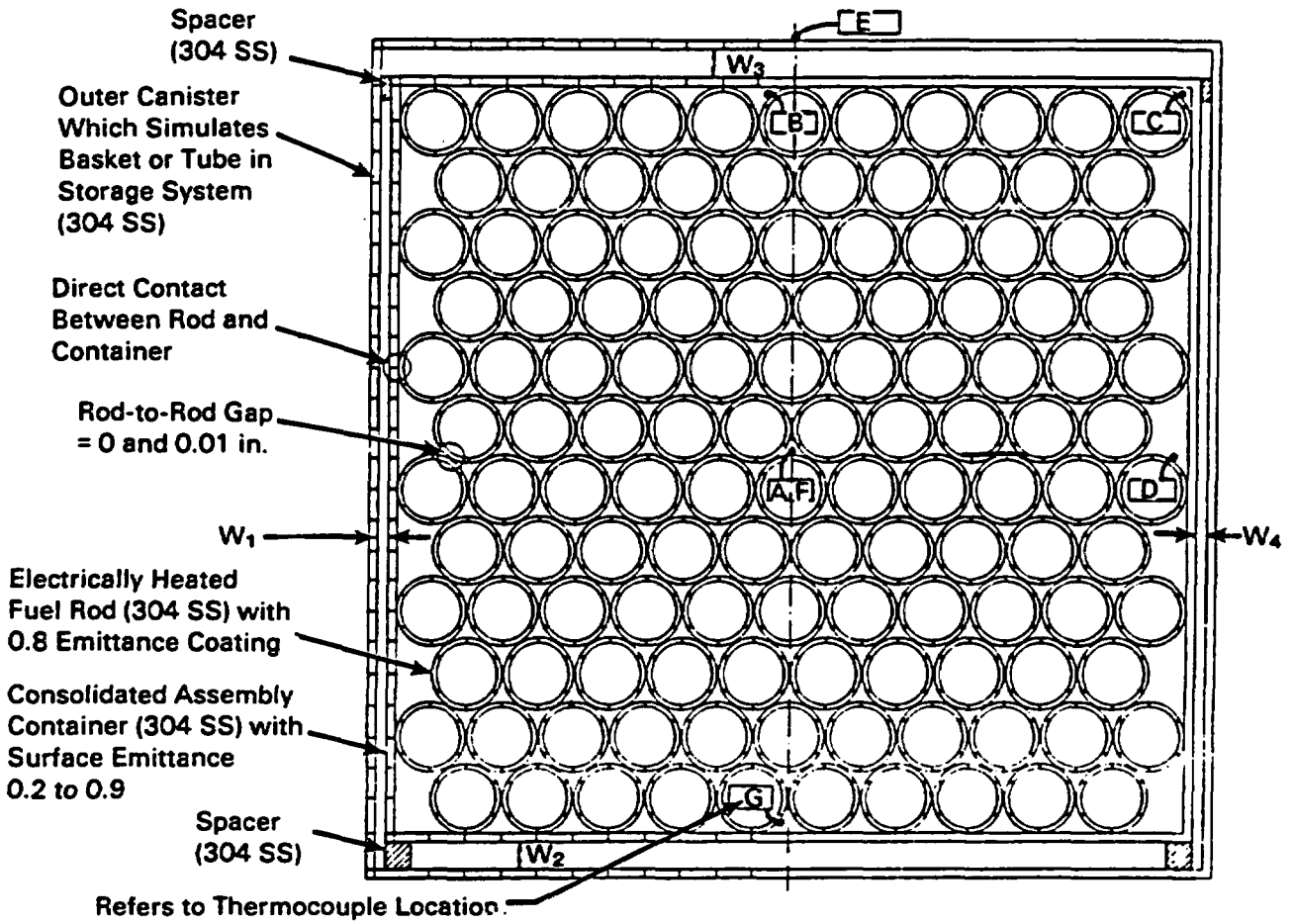

FIGURE 4.3. Consolidated Assembly Test Section

filled with two-hole ceramic insulators containing Nichrome™ heater wire to provide a uniform heat generation profile along the full 24-in. length. The insulator material was mullite, an aluminum silicate ($3Al_2O_3$-SiO_2). Wire wraps at each end of the tube centered the mullite in the tube with a nominal gap of 0.050 in. between the ceramic and the inner surface of the tube. The emittance of the outer surface of the stainless steel tube was altered by black nickel plating. This produced a surface emittance reported to be approximately 0.8 (Eggers 1985a), a value consistent with the emittance of actual spent fuel rods.

The radial locations of the thermocouples used to measure the temperatures in this test section are also shown in Figure 4.3. The boundary temperature was measured only on the top surface of the test section (E) and at the center of each end of the test section (thermocouples H2 and H3, not shown in Figure 4.3). Thermocouples were located at the radial positions indicated in Figure 4.3 at three axial levels along the assembly. The boundary temperature thermocouples (labeled E in Figure 4.3) were located at Planes A, B, and C (the same locations used in the unconsolidated test section; see Figure 4.2). The thermocouples on the rods were located at three different axial positions in one half of the test section. Plane 1 was the midplane of the test section, Plane 2 was 9 in. from the end of the test section, and Plane 3 was 6 in. from the same end of the test section. Figure 4.2 shows the relative axial locations of these measurement planes.

The test matrix for the consolidated rod tests is shown in Table 4.2. The first seven tests (1, 2, and 4 through 8) used rods that were in contact with a nominal zero rod-to-rod gap. Air and helium atmospheres were used with equivalent power levels of 100 W, 400 W, and 800 W. The actual power levels for the 24-in. test section were 1/6 of the equivalent assembly power levels. Another five tests (designated as 11, 12, 14, 16, and 18) used rods that were separated by 0.01 in. using shims at each end of the test section. The gaps (W_1, W_2, W_3, and W_4) between the inner canister and outer fuel tube

---

™ Special nickel chromium alloy used for resistance wire and strip, manufactured by Driver-Harris Company, Harrison, New Jersey.

TABLE 4.2. Consolidated Assembly Test Matrix

Test	Internal Atmosphere	Equivalent Decay Heat Level Per Consolidated Canister, Watts	Rod-to-Rod Gap, Inches	Annular Gap,[a] Mils W_1	W_2	W_3	W_4	Emittance[b] Fuel Rods	Canister Outer Surface	Fuel Tube Inner Surface
1	Air	100	0.0	20-40	100-120	100-120	20-40	0.7-0.8	0.2-0.3	0.2-0.3
2	Air	400	0.0	20-40	100-120	100-120	20-40	0.7-0.8	0.2-0.3	0.2-0.3
4	Air	800	0.0	20-40	100-120	100-120	20-40	0.7-0.8	0.2-0.3	0.2-0.3
5	Helium	100	0.0	20-40	100-120	100-120	20-40	0.7-0.8	0.2-0.3	0.2-0.3
6	Helium	400	0.0	20-40	100-120	100-120	20-40	0.7-0.8	0.2-0.3	0.2-0.3
7	Helium	400	0.0	20-40	100-120	100-120	20-40	0.7-0.8	0.2-0.3	0.2-0.3
8	Helium	800	0.0	20-40	100-120	100-120	20-40	0.7-0.8	0.2-0.3	0.2-0.3
11	Air	100	0.01	30-50	70-90	70-90	30-50	0.7-0.8	0.2-0.3	0.2-0.3
12	Air	400	0.01	30-50	70-90	70-90	30-50	0.7-0.8	0.2-0.3	0.2-0.3
14	Air	800	0.01	30-50	70-90	70-90	30-50	0.7-0.8	0.2-0.3	0.2-0.3
16	Helium	400	0.01	30-50	70-90	70-90	30-50	0.7-0.8	0.2-0.3	0.2-0.3
18	Helium	800	0.01	30-50	70-90	70-90	30-50	0.7-0.8	0.2-0.3	0.2-0.3
S-1	Air	400	0.0	80-100	240-260	20-40	20-40	0.7-0.8	0.2-0.3	0.2-0.3
S-2	Air	800	0.0	80-100	240-260	20-40	20-40	0.7-0.8	0.2-0.3	0.2-0.3
S-3	Helium	400	0.0	80-100	240-260	20-40	20-40	0.7-0.8	0.2-0.3	0.2-0.3
S-4	Helium	800	0.0	80-100	240-260	20-40	20-40	0.7-0.8	0.2-0.3	0.2-0.3
S-5	Vacuum (air)	400	0.0	20-40	100-120	100-120	20-40	0.7-0.8	0.2-0.3	0.2-0.3
S-7	Air	400	0.0	20-40	100-120	100-120	20-40	0.7-0.8	0.8-0.9	0.8-0.9
S-8	Air	800	0.0	20-40	100-120	100-120	20-40	0.7-0.8	0.8-0.9	0.8-0.9
S-9	Helium	400	0.0	20-40	100-120	100-120	20-40	0.7-0.8	0.8-0.9	0.8-0.9
S-10	Helium	800	0.0	20-40	100-120	100-120	20-40	0.7-0.8	0.8-0.9	0.8-0.9

(a) Annular gaps varied between high and low values due to bow and bend of canister and storage tube; aluminum shim plates were used to attempt to maintain gap size in similar range.

(b) Emittance ranges based on vendor-supplied data or published values.

(refer to Figure 4.3) were somewhat different because of the increased gap between rods. The results of these tests are documented in Eggers (1985a).

Nine additional tests were performed to assess the effects of an assembly that is eccentric to the center of the fuel tube and to study the effect of increasing the emittances of the outer canister surface and inner fuel tube surface. Tests S-1 through S-4 used an eccentric assembly with air and helium atmospheres and equivalent power levels of 400 W and 800 W. Tests S-5 and S-7 through S-10 used increased emittances for the canister and fuel tube but were otherwise similar to tests 1 through 8 as indicated in Table 4.2. This series of tests and the resulting data are discussed in detail in Eggers (1985a).

5.0 MODELING UNCERTAINTIES

Typical spent fuel storage casks and canisters containing spent fuel assemblies are complex hydrothermal systems, and some uncertainty about how best to construct an accurate overall model will always be present. These uncertainties lead inevitably to approximations, some of which may be difficult to quantify. Most uncertainties may be placed within one of three broad categories:

1. basic information that is application-specific and measurable (e.g., container dimensions, heat generation rates, ambient conditions)
2. information generic to most applications (e.g., property values, correlations)
3. decisions about how to achieve the best match between a particular code and the application (e.g., computational mesh, internal algorithms).

Some of the more important factors falling within these categories are:

- The information shown on the furnished drawings may be incomplete or may not accurately reflect the as-built structure.
- Dimensional tolerances may be particularly significant when they influence small gaps with important thermal resistances. The input to HYDRA-II specified dimensions falling within the estimated range.
- Potential eccentricities, such as the actual placement of the fuel rods within the container, are a source of uncertainty. The input to HYDRA-II specified eccentricities within the estimated range.
- The total heat generation rate and the generation rate spatial profiles have a direct impact on predicted cladding temperatures.
- All material property values possess a range of uncertainty, although the range for most well-characterized materials is usually not significant. Exceptions include the emittance of some

materials, especially if the surface has been altered by some process (e.g., cladding corrosion or basket structure sandblasting). The HYDRA-II input file specified values believed to be typical. The potential consequences of a range of values on the temperature field have not been investigated.

- Some boundary conditions may be difficult to determine. An example is sparse temperature data for the external canister body.
- Some uncertainties are inherent in the use of discrete solution methods. An example is the trade-off between mesh coarseness and accuracy. The conservation equations have been formulated within HYDRA-II in an entirely consistent fashion. Basically, this means that any desired numerical accuracy may be achieved by using a sufficiently large number of computational cells. The practical trade-off is between accuracy and computer time and costs. The optimum is difficult to determine a priori.
- Another source of uncertainty results from limitations of models constructed internal to the code. Thermal radiation models are a good example. All radiation enclosures within a cask, assembly, or canister are three-dimensional. Two-dimensional radiation models are used extensively within HYDRA-II for practical reasons. The errors associated with this approximation can be reduced, but not eliminated, by careful selection of a computational mesh.

Finally, there is a fourth category of uncertainty not mentioned previously--human error. The internal coding or input specifications intended may not be what is actually present. This situation is at its worst when the offending mistake results in an error that is both significant and unobtrusive.

6.0 COMPUTATIONAL METHODOLOGY AND RESULTS

Input models were constructed for the HYDRA-II code to describe the test sections containing the unconsolidated and consolidated rod assemblies. These input models consisted of geometric descriptions of the test sections, parameters modeling the heat transfer due to thermal radiation and conduction, and specification of the boundary conditions. The computational methodology and results for the unconsolidated rods and consolidated rods are discussed, respectively, in Sections 6.1 and 6.2. Section 6.2 concludes with the results of a simulation showing how temperatures might be affected for a consolidated fuel assembly that touches one side of a fuel tube.

6.1 UNCONSOLIDATED ASSEMBLY

The test section for unconsolidated rods was described in Section 4.1. The computational mesh and material properties used to model the physical test section are described here. Section 6.1 concludes with a discussion of predictions compared to experimental data.

6.1.1 Computational Methodology

A transverse cross section of the unconsolidated assembly was shown in Figure 4.1. Figure 6.1 shows the corresponding computational mesh employed, and indicates the alignment of mesh with various physical features of the assembly test section. A single layer of computational cells in the transverse plane was used to model the test section midplane.

The HYDRA-II code generally computes a temperature and three mass fluxes (if convection is present) corresponding to each computational cell. However, in this application, convection was insignificant compared to conduction and thermal radiation heat transfer, so mass fluxes were not computed. The shape and location of each cell were selected, insofar as practical, to coincide with physical structures or boundaries of the fuel tube and its contents, because the accuracy of predictions is influenced significantly by how well the computational mesh is aligned with the physical structure.

Thermophysical properties were obtained from Eggers Ridihalgh Partners (Eggers 1985b) and Touloukian and Ho (1970). The properties used for all

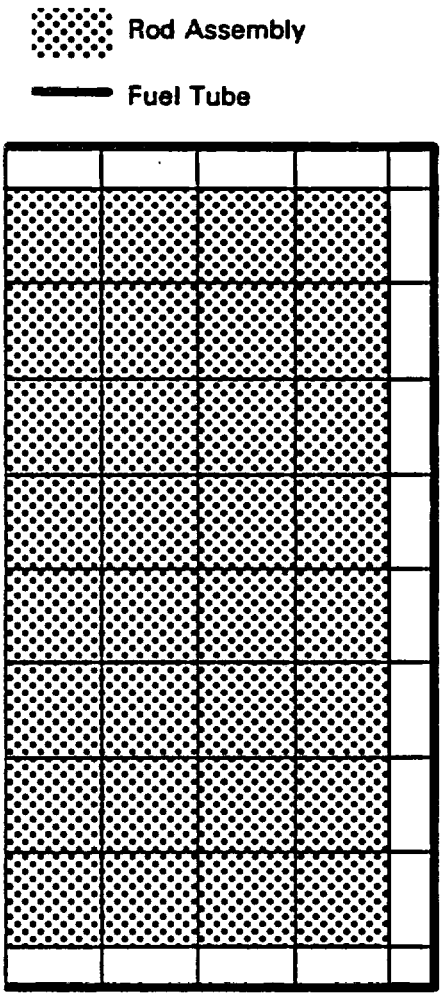

FIGURE 6.1. Transverse Computational Mesh and Its Alignment with Unconsolidated Test Section Physical Features

simulations are listed in Table 6.1. Effective thermal conductivities were computed for those computational cells containing more than one material. In the simulation denoted as vacuum, the actual backfill was air at low pressure. However, the pressure was high enough so that the mean free path of the gas was less than any significant lengths (gaps). The properties used for the vacuum simulations were therefore those of air.

The effective thermal conductivity in the axial direction of the rod assembly was greater than 60 times that in the transverse direction. The ratio of axial to transverse length of the test section was approximately 4 (24 in./6 in.). This relatively high thermal conductivity in the axial

TABLE 6.1. Thermophysical Properties Used in Unconsolidated Assembly Simulations

Material	Thermal Conductivity, W/cm°K
Aluminum	1.779
Mullite	5.0 E-2
Air	0.688E-4 + (0.634E-6)T
	Emittance
Rods	0.85
Fuel tube	0.25

direction allows the potential for substantial heat loss from the ends of the test section. A heat transfer coefficient accounting for convection and thermal radiation from the ends of the test section was assumed in the simulation because this information was not provided in the test documentation (Eggers 1985b).

6.1.2 Predictions Compared to Data

Two test cases were selected for simulation: 1) case U1, air atmosphere, 401 W decay heat rate, and 2) case U5-A, vacuum (air) atmosphere, 809 W decay heat rate. These two test cases include the two nominal decay heat rates (400 W and 800 W) used in the experiments. Other test cases had slightly different boundary temperatures and therefore provide little additional information.

The HYDRA-II predictions were then compared to the actual test data. The results are shown in tabular form in Table 6.2 and graphically in

TABLE 6.2. HYDRA-II-Predicted Temperatures Compared to Test-Measured Temperatures for Unconsolidated Assembly Test Section

Case	Internal Atmosphere	Equivalent Decay Heat Level per Unconsolidated Assembly, Watts		Temperature, °C Fuel Tube	Rod Location 1	2	3
U1	Air	401	Data	180	200	194	189
			Predictions	180	204	195	189
U5-A	Vacuum (air)	809	Data	196	246	230	221
			Predictions	196	245	227	216

Figure 6.2. Overall, the predictions and data are in generally good agreement. The largest discrepancy between predictions and data is 5°C, approximately the same as the average scatter in the experimental data. Despite the good agreement between predictions and data, the results may be subject

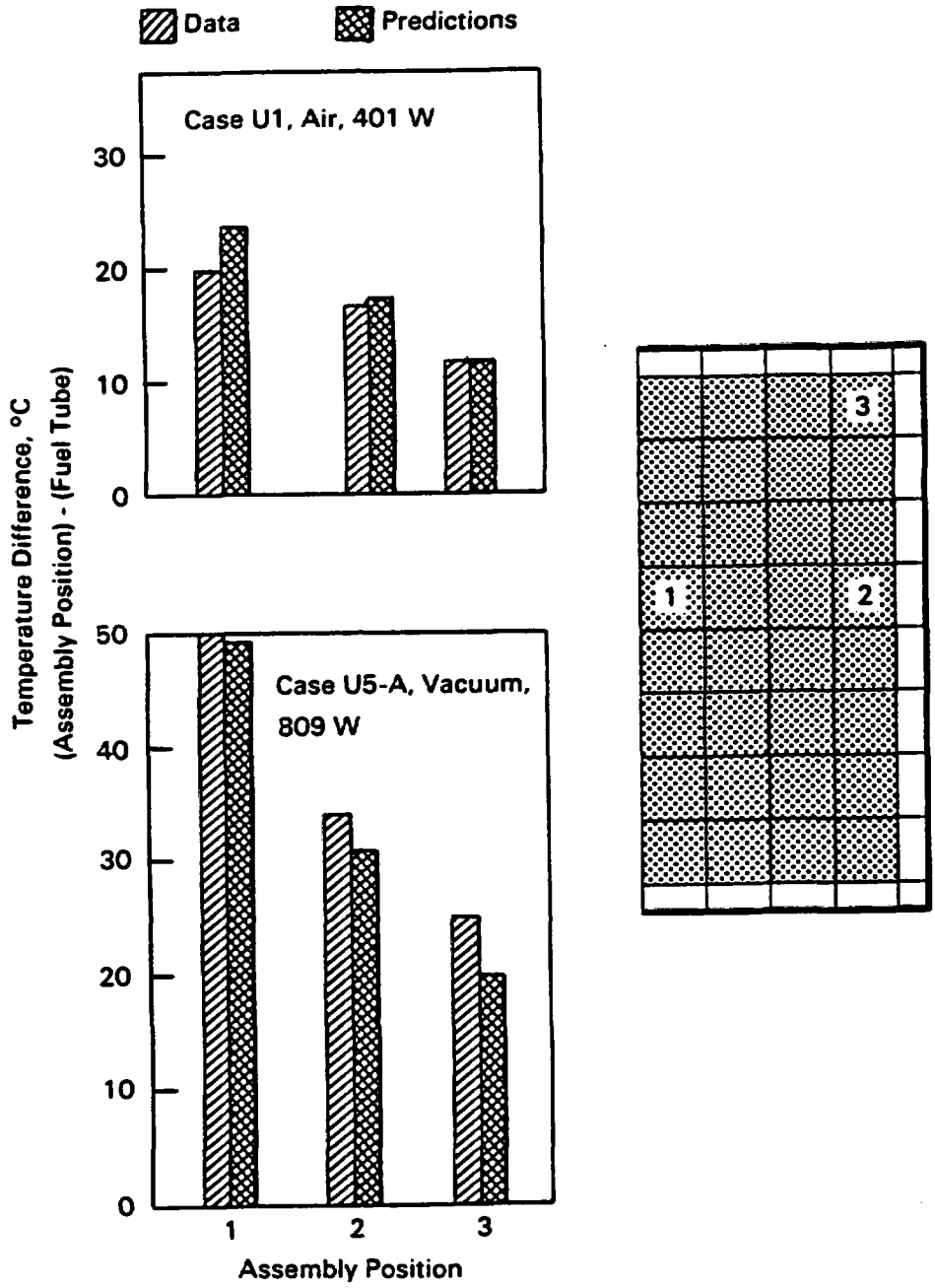

FIGURE 6.2. HYDRA-II-Generated Temperature Predictions Compared to Test-Measured Temperature for Unconsolidated Assembly Test Section

to question. The reason is that rod temperatures are very sensitive to the substantial heat loss from the ends of the test section. The test documentation provided no information to ensure that the heat losses assumed in the simulations were those that actually occurred.

6.2 CONSOLIDATED ASSEMBLY

The consolidated rod test section was described in Section 4.2. The computational mesh and material properties used to model that test section are presented in the following paragraphs. The HYDRA-II-generated predictions are then compared to experimental data. Predictions for a rod assembly that is eccentric within a fuel tube conclude this section.

6.2.1 Computational Methodology

The consolidated assembly test section was shown in Figure 4.3. Figure 6.3 depicts the corresponding computational mesh employed and indicates its alignment with various physical features of the test section. A single layer of computational cells in the transverse plane was used to model the midplane of the test section.

As with the unconsolidated assembly simulation, mass fluxes were not computed because convection was insignificant compared to conduction and thermal radiation heat transfer. Again, each cell's shape and location were selected, insofar as practical, to coincide with physical structures or boundaries of the fuel tube and its contents, to enhance prediction accuracy.

Thermophysical properties were obtained from Eggers (1985b) and Touloukian and Ho (1970). The properties used for all simulations are listed in Table 6.3. Effective thermal conductivities were computed for those computational cells containing more than one material.

6.2.2 Predictions Compared to Data

Six test cases were selected for simulation; they include two decay heat rates (400 W and 800 W), two backfill gases (air and helium), and the two rod-to-rod gaps (0.0 in. and 0.01 in.). The HYDRA predictions were then compared to the measured temperatures obtained in the tests.

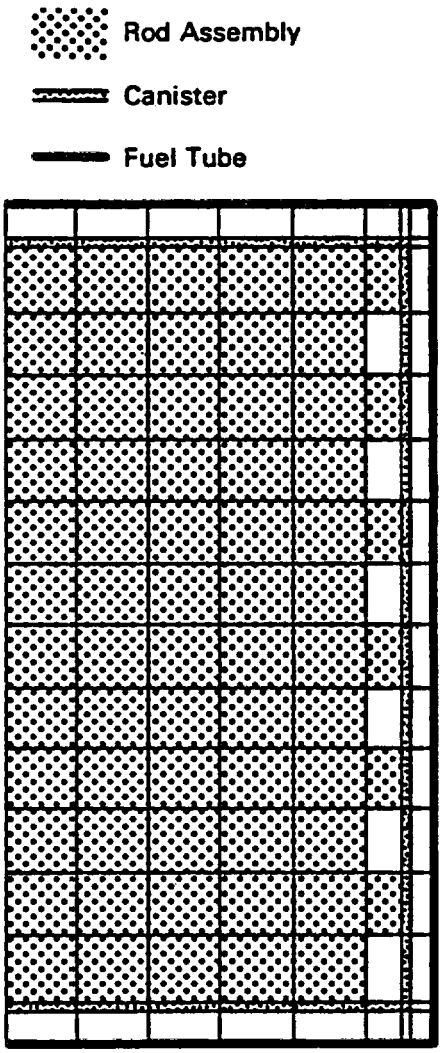

FIGURE 6.3. Transverse Computational Mesh and Its Alignment with Consolidated Test Section Physical Features

The results of the comparisons are shown in Table 6.4. The rod locations referred to in Table 6.4 are shown graphically as part of Figures 6.4 through 6.6. The agreement between predictions and data is very good. The mean deviation for the 30 temperature comparisons is ±0.03°C; the standard deviation (root-mean-square error) is ±2.5°C. The largest discrepancy is 5°C. The test documentation (Eggers 1985b) indicates uncertainty limits of ±2.1°C for measured temperature differences as well as other sources of uncertainty, some of which are difficult to quantify. If there are any trends in the discrepancy between predictions and data, they cannot be separated from data scatter.

TABLE 6.3. Thermophysical Properties Used in Consolidated Assembly Simulations

Material	Thermal Conductivity, W/cm°K
Stainless Steel	0.9215E-1 + (0.1465E-3)T
Mullite	5.0E-2
Air	0.688E-4 + (0.634E-6)T
Helium	0.52E-3 + (0.32E-5)T
	Emittance
Rods	0.8
Canister	0.25
Fuel tube	0.25

There are, however, clearly discernible trends that relate to different test parameters. The separate effects of changing power levels, backfill gases, and rod-to-rod gaps are illustrated, respectively, in Figures 6.4 through 6.6.

Figure 6.4 shows the effect of doubling the equivalent power level from 400 W to 800 W (backfill gas and rod-to-rod gap held constant). Doubling the power approximately doubles the temperature rise above the fuel tube temperature. The temperature rise would be exactly proportional to the power level, were it not for temperature-dependent thermal conductivities and the nonlinearity of thermal radiation. If significant convection were present, then an additional nonlinearity would be introduced.

Figure 6.5 shows the effect of helium and air backfill gases. The thermal conductivity of helium is about 2.0E-3 W/cm°K, and that of air is about 3.7E-4 W/cm°K at the test temperatures. The temperature differences are smaller for the helium backfill gas (compared to air), but not by a factor of 5 because the thermal conductivities of the assembly material components remain relatively unchanged.

Figure 6.6 shows the effect of varying the rod-to-rod gaps from 0.0 in. to 0.01 in. The two gaps are nominal due to slight bowing of the rods and the difficulty of stacking rods in a precisely hexangular array. The assembly centerline temperature difference (temperature above the fuel tube) is

TABLE 6.4. HYDRA-Predicted Temperatures Compared to Test-Measured Temperatures for Consolidated Assembly Test Section

Case	Internal Atmosphere	Equivalent Decay Heat Level per Consolidated Assembly, Watts	Rod-to-Rod Gap, Inches		Temperature, °C					
					Fuel Tube	Rod Location A	B	C	D	G
2	Air	400	0.0	Data	195	207	204	201	201	202
				Predictions	195	209	206	202	204	206
4	Air	800	0.0	Data	195	224	216	211	214	215
				Predictions	195	222	216	210	212	216
8	Helium	800	0.0	Data	191	206	201	198	199	199
				Predictions	191	202	198	194	196	198
12	Air	400	0.01	Data	197	213	208	205	204	202
				Predictions	197	214	207	203	205	207
14	Air	800	0.01	Data	192	225	214	209	207	210
				Predictions	192	225	213	205	210	213
18	Helium	800	0.01	Data	193	206	201	197	194	195
				Predictions	193	206	199	195	198	199

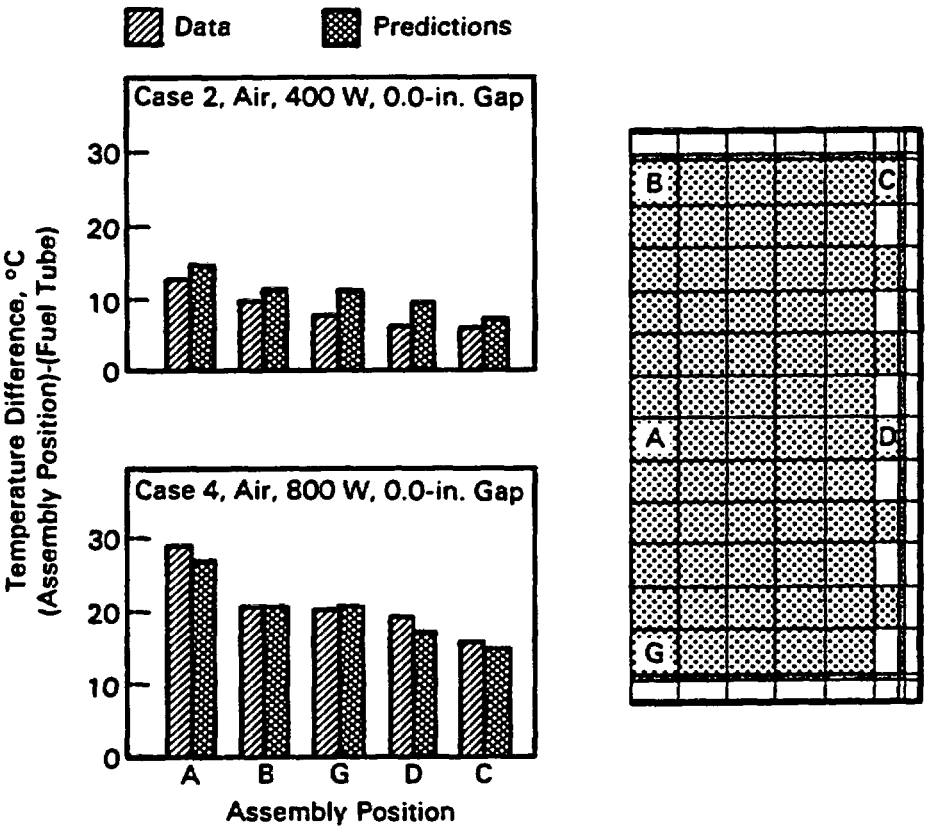

Figure 6.4. HYDRA-II-Predicted Temperatures Compared to Test-Measured Temperatures for Two Power Levels

27°C for the 0.0-in. gap case and 33°C for the 0.01-in. gap case. This is approximately a 20% increase in centerline temperature for a 0.01-in. gap increase. Note that this result applies to an air backfill and the specific test section conditions. Also note that the gaps between the canister and fuel tube were not identical for cases 4 and 14, as shown in Table 4.2. In any event, it appears that no severe penalty is associated with a loosely packed assembly of rods.

6.2.3 Temperature Predictions for Assembly Eccentric to Fuel Tube

The results presented thus far have been for a rod assembly symmetrically positioned within the fuel tube. The effect, if any, on rod temperatures when a rod assembly is displaced to one side of a fuel tube was also examined in this analysis. An eccentric assembly is the usual case in practice, whether the rods are unconsolidated or consolidated, even when the assembly axis is vertical.

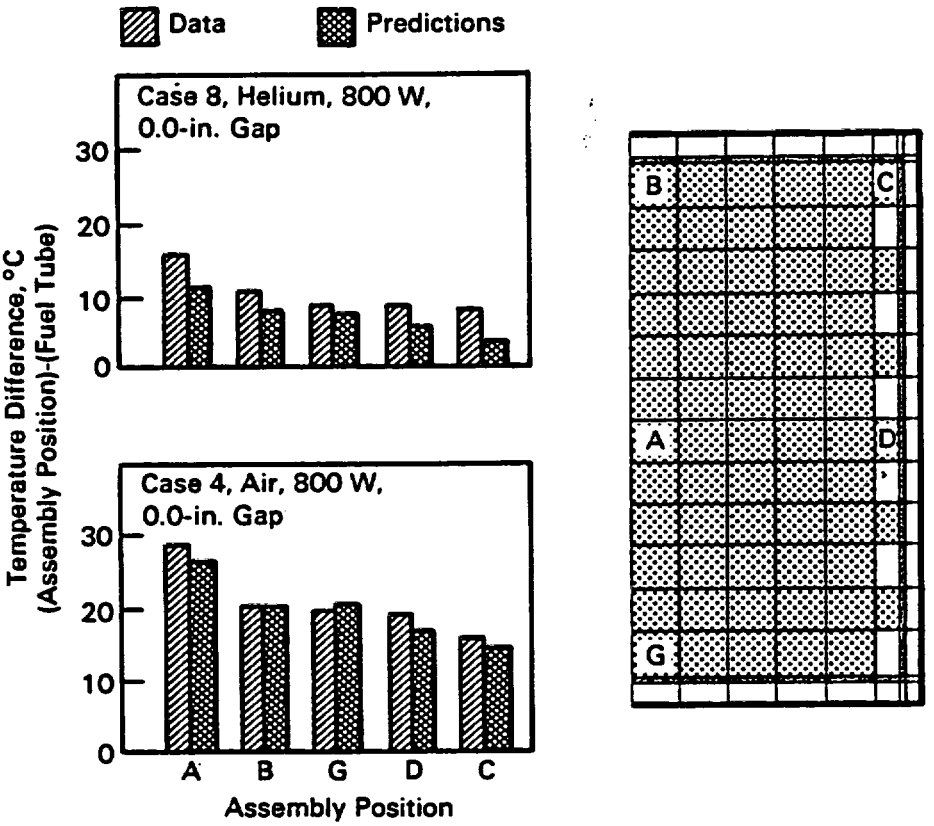

FIGURE 6.5. HYDRA-II-Predicted Temperatures Compared to Test-Measured Temperatures for Two Backfill Gases

Four experimental tests (Tests S-1 through S-4 shown in Table 4.2) were conducted with an eccentric consolidated assembly (Eggers 1985a). Unfortunately, dissimilar boundary conditions and data scatter make it difficult to discern any trends. However, it is easy to simulate an eccentric assembly.

Case 14 previously simulated was selected for a different HYDRA-II simulation that introduced eccentricity. This case had an air atmosphere, 800 W of power, and a 0.01-in. rod-to-rod gap. The space between the canister and fuel tube was 0.08 in. at the top and bottom of the canister (W_2 and W_3 shown in Figure 4.3 and listed in Table 4.2). In the eccentric case, the bottom space (W_2) was reduced to 0.005 in. and the top space (W_3) proportionally increased to 0.155 in. All other parameters remained unchanged.

Results for the centered and eccentric cases are compared in Figure 6.7. The temperature profiles shown are along the vertical centerline of the

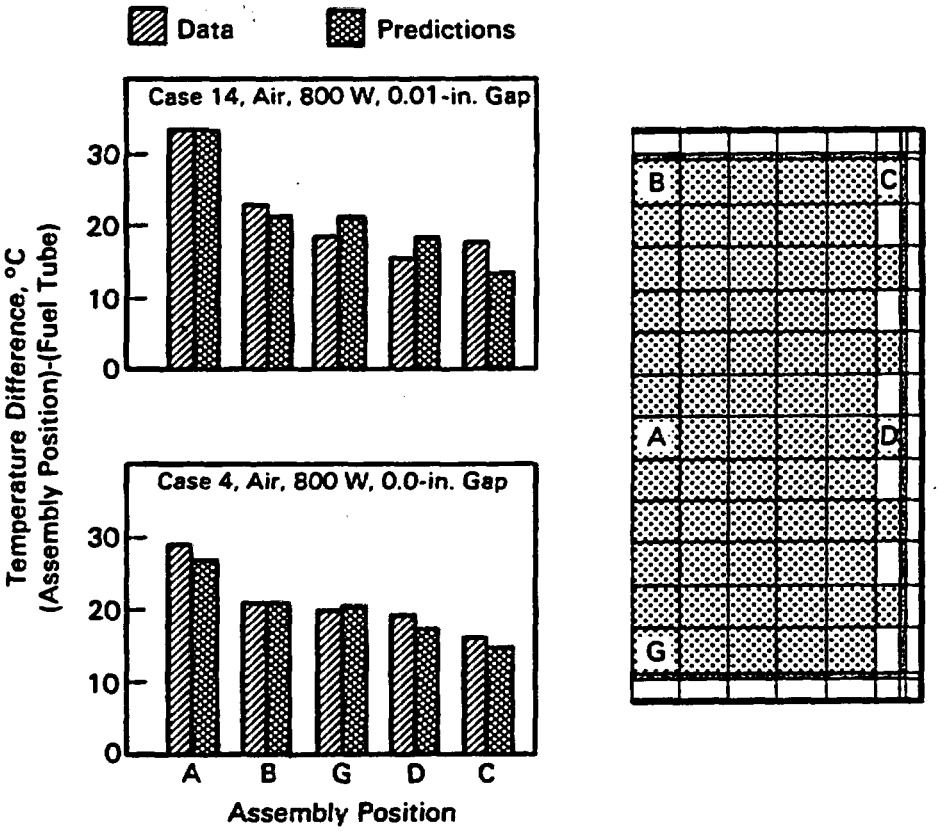

FIGURE 6.6. HYDRA-II-Predicted Temperatures Compared to Test-Measured Temperatures for Two Rod-to-Rod Gaps

transverse cross section. The centered case exhibits a symmetric temperature profile with temperatures in the lower half of the assembly, mirroring those in the upper half. The eccentric case shows generally lower temperatures in the lower half of the assembly compared to those in the upper half. The peak cladding temperature is 3°C (approximately 10%) lower for the eccentric case compared to the centered case.

The fuel tube temperature is the same for both cases. Under this condition, more heat leaves the eccentric assembly across the narrow space at the bottom than at the top. In practice, the fuel tube (and rod assembly) is part of a larger structure, and excess flow of heat to a portion of the fuel tube would tend to raise the temperature. The two curves shown in Figure 6.7 can be regarded as limiting cases.

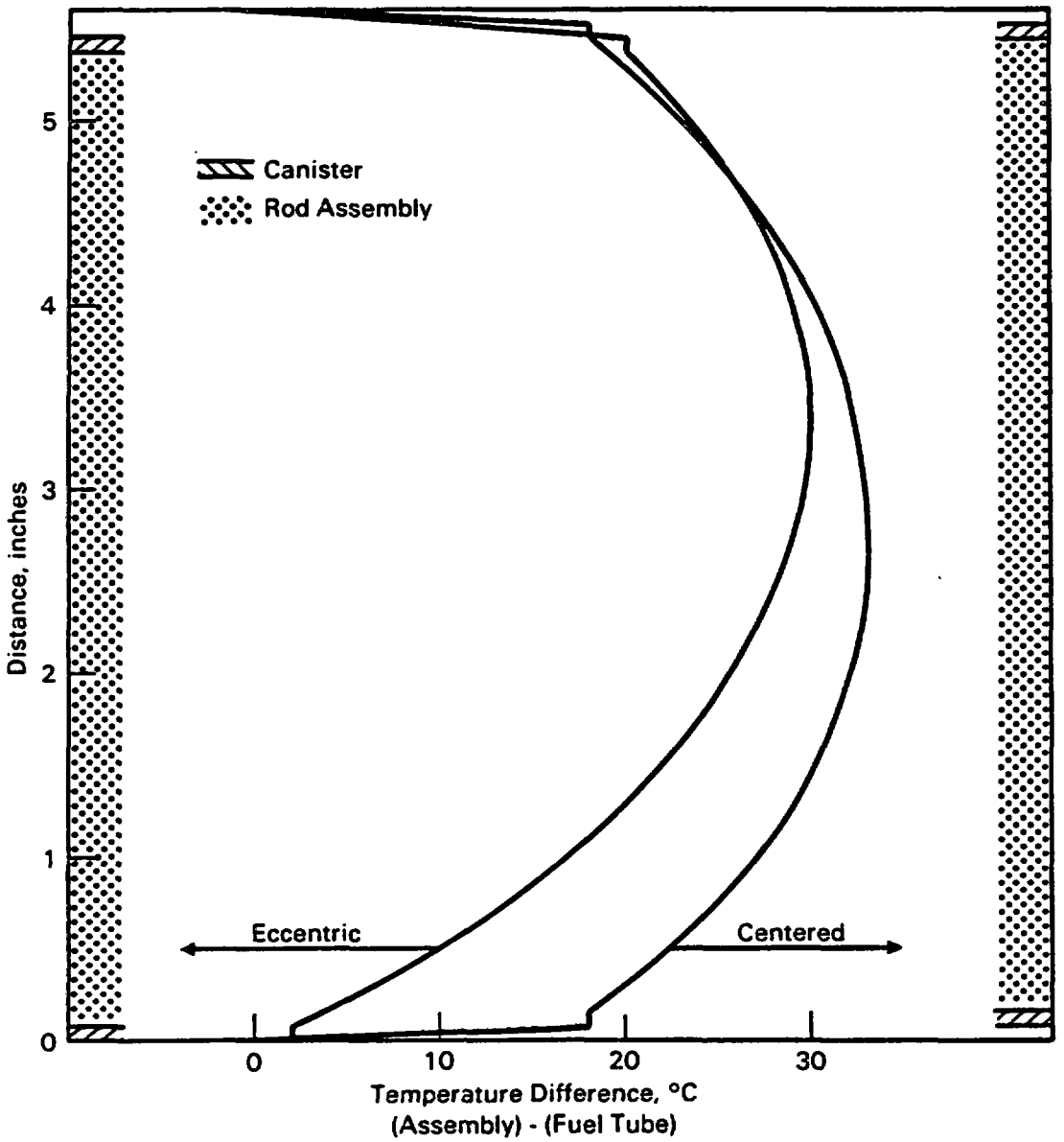

FIGURE 6.7. HYDRA-II-Predicted Vertical Centerline Temperature Profiles for Centered and Eccentric Rod Assemblies

7.0 REFERENCES

Creer, J. M., R. A. McCann, M. A. McKinnon, J. E. Tanner, E. R. Gilbert, and R. L. Goodman. 1986. The Castor-V/21 PWR Spent-Fuel Storage Cask: Testing and Analyses. EPRI NP-4887, Electric Power Research Institute, Palo Alto, California.

Douglas, J., and J. Gunn. 1964. "A General Formulation of Alternating Direction Methods." I. Numer. Math. 6:428.

Eggers, P. E. 1985a. Thermal Testing of Simulated BWR Consolidated Fuel. EPRI-NP-4119, Electric Power Research Institute, Palo Alto, California.

Eggers, P. E. 1985b. Thermal Test Results for Simulated BWR Unconsolidated and Consolidated Fuel. Eggers Ridihalgh Partners, Inc., Columbus, Ohio.

McCann, R. A. 1986. Comparison of HYDRA Predictions to Temperature Data from Two Single-Assembly Spent Fuel Heat Transfer Tests. PNL-6074, Pacific Northwest Laboratory, Richland, Washington.

McCann, R. A. 1987. HYDRA-II: A Hydrothermal Analysis Computer Code, Volume I - Equations and Numerics. PNL-6206 Vol. I, Pacific Northwest Laboratory, Richland, Washington.

McCann, R. A., and P. S. Lowery. 1987. HYDRA-II: A Hydrothermal Analysis Computer Code, Volume III - Verification/Validation Assessments. PNL-6206 Vol. III, Pacific Northwest Laboratory, Richland, Washington.

McCann, R. A., P. S. Lowery, and D. L. Lessor. 1987. HYDRA-II: A Hydrothermal Analysis Computer Code, Volume II - Users Manual. PNL-6206 Vol. II, Pacific Northwest Laboratory, Richland, Washington.

Patankar, S. V. 1980. Numerical Heat Transfer and Fluid Flow. Hemisphere Publishing Corp., Washington, D.C.

Raithby, G. D., and G. E. Schneider. 1979. "Numerical Solution of Problems in Incompressible Fluid Flow: Treatment of Velocity-Pressure Coupling." Numer. Heat Transfer 2:417-440.

Raithby, G. D., and G. E. Schneider. 1980. "Erratum." Numer. Heat Transfer 3:513.

Touloukian, Y. S., and C. Y. Ho. 1970. Thermophysical Properties of Matter. Thermophysical Properties Research Center, Purdue University, West Lafayette, Indiana.

U.S. Department of Energy. 1986. Spent Fuel Storage Requirements. DOE/RL-86-5, U.S. Department of Energy Richland Operations Office, Richland, Washington.

Wiles, L. E., N. J. Lombardo, C. M. Heeb, U. P. Jenquin, T. E. Michener, C. L. Wheeler, J. M. Creer, and R. A. McCann. 1986. BWR Spent Fuel Storage Cask Performance Test: Volume II - Pre- and Post-Test Decay Heat, Heat Transfer, and Shielding Analyses. PNL-5777 Vol. II, Pacific Northwest Laboratory, Richland, Washington.

DISTRIBUTION

No. of Copies

82 DOE/Office of Scientific and Technical Information

L. Barrett
U.S. Department of Energy
Office of Civilian Radioactive Waste Management
RW-33
Washington, DC 20585

G. Hartkopf
U.S. Department of Energy
Office of Civilian Radioactive Waste Management
RW-32
Washington, DC 20585

K. A. Klein
U.S. Department of Energy
Office of Civilian Radioactive Waste Management
RW-32
Washington, DC 20585

D. E. Shelor
U.S. Department of Energy
Office of Civilian Radioactive Waste Management
RW-32
Washington, DC 20585

E. L. Wilmot
U.S. Department of Energy
Office of Civilian Radioactive Waste Management
RW-33
Washington, DC 20585

J. S. Finucane
U.S. Department of Energy
Energy Information Administration
EI-53
Washington, DC 20585

No. of Copies

M. Fisher
U.S. Department of Energy
Idaho Operations Office
785 DOE Place
Idaho Falls, ID 83402

S. T. Hinschberger
U.S. Department of Energy
Idaho Operations Office
785 DOE Place
Idaho Falls, ID 83402

K. G. Golliher
U.S. Department of Energy
Albuquerque Operations Office
P.O. Box 5400
Albuquerque, NM 87115

C. J. Daukowski
U.S. Department of Energy
Attention: Defense Programs
San Francisco Operations Office
1333 Broadway
Oakland, CA 94612

C. Matthews
U.S. Department of Energy
Oak Ridge National Laboratory
P.O. Box E
Oak Ridge, TN 37830

C. Gertz
U.S. Department of Energy
Nevada Operations Office
P.O. Box 98518
Las Vegas, NV 89193-8588

N. H. Davison
U.S. Nuclear Regulatory Commission
Office of Nuclear Materials Safety and Safeguards
Washington, DC 20555

No. of
Copies

C. Feldman
U.S. Nuclear Regulatory
Commission
Office of Nuclear Regulatory
Research
MS 1130-SS
Washington, DC 20555

C. H. Peterson
U.S. Nuclear Regulatory
Commission
Office of Nuclear Material
Safety and Safeguards
MS 623-SS
Washington, DC 20555

J. Roberts
U.S. Nuclear Regulatory
Commission
Office of Nuclear Material
Safety and Safeguards
MS 396-SS
Washington, DC 20555

L. C. Rouse
U.S. Nuclear Regulatory
Commission
Office of Spent Fuel
Storage Installation
Division of Fuel Cycle and
Material Safety
Washington, DC 20555

J. A. Carr
Battelle Memorial Institute
Office of Nuclear Waste
Isolation
505 King Avenue
Columbus, OH 43201

Technical Library
Battelle Memorial Institute
Office of Nuclear Waste
Isolation
505 King Avenue
Columbus, OH 43201

No. of
Copies

L. J. Jardine
Bechtel National, Inc.
Advanced Technology Division
P.O. Box 3965
San Francisco, CA 94119

R. Kunita
Carolina Power & Light Co.
P.O. Box 1551
Raleigh, NC 27602

C. K. Anderson
Combustion Engineering, Inc.
1000 Prospect Hill Road
Windsor, CT 06095

T. Grant
Ebasco Services Incorporated
Two World Trade Center
New York, NY 10048

P. E. Eggers
Eggers Ridihalgh Partners, Inc.
1445 Summit Street
Columbus, OH 43201

FLUOR Engineers, Inc.
Advanced Technology Division
3333 Michelson Drive
Irvine, CA 92730

R. Anderson
General Nuclear Services, Inc.
135 Darling Drive
Avon, CT 06001

L. B. Ballou
Lawrence Livermore National
Laboratory
P.O. Box 808
Livermore, CA 94550

M. W. Schwartz
Lawrence Livermore National
Laboratory
P.O. Box 808
Livermore, Ca 94550

No. of
Copies

C. E. Walter
Lawrence Livermore National
Laboratory
P.O. Box 808
Livermore, Ca 94550

H. Lowenberg
Lowenberg Associates
10901 Rosemont Drive
Rockville, MD 20852

J. Houston
Nuclear Assurance Corporation
6251 Crooked Creek Road #200
Norcross, GA 30092-3107

P. A. Craig
Nuclear Packaging Inc.
1010 S. 336th Street
Federal Way, WA 98003

L. E. Wiles
Numerical Applications, Inc.
825 Goethals Drive
Richland, WA 99352

C. L. Wheeler
Numerical Applications, Inc.
825 Goethals Drive
Richland, WA 99352

B. Lehnert
NUTECH Engineers
145 Martinvale Lane
San Jose, CA 95116

C. V. Parks
Oak Ridge National Laboratory
P.O. Box X
Oak Ridge, TN 37831

D. Woods
Ralph M. Parsons Co.
100 West Walnut Street
Pasadena, CA 91124

No. of
Copies

J. V. Massey
Reedy and Associates
103 Albright Way
Los Gatos, CA 95030

T. L. Sanders
Sandia National Laboratory
P.O. Box 5800
Albuquerque, NM 87115

M. E. Mason
Transnuclear, Inc.
Two Skyline Drive
Hawthorne, NY 10532-2120

TRW Exploration/PRO
P.O. Box 441807
Houston, TX 77244-1807

M. L. Smith
Virginia Power Co.
5000 Dominion Blvd.
Glen Allen, VA 23060

K. L. Basehore
Virginia Electric and Power Co.
Power Station Engineering
The Electric Building
P.O. Box 564
7th and Franklin
Richmond, VA 23204

D. L. Larkin
Washington Public Power Supply
System
P.O. Box 968
Richland, WA 99352

R. O. Anderson
Northern States Power Company
15 S. 15th Street
Minneapolis, NM 55401

G. Swindlehurst
Duke Power Company
P.O. Box 33189
422 S. Church Street
Charlotte, NC 28242

No. of
Copies

D. Hamilton
Middle South Services, Inc.
Box 61000
New Orleans, LA 70161

G. R. Bond
Manager, Nuclear Fuels
General Public Utilities, NUC
100 Interpace Parkway
Parsippany, NJ 07054

J. R. Ratliff
Tennessee Valley Authority
409 Krystal Building
Chattanooga, TN 37401

B. Rice
Texas Utilities Generating Co.
Skyway Tower
400 North Olive Street
LD81
Dallas, TX 75201

H. E. Bliss
Nuclear Fuel Services
Commonwealth Edison
72 West Adams Street
P.O. Box 767
Chicago, IL 60690

R. T. Harris
Northeast Utilities Service Co.
P.O. Box 270
Hartford, CT 06101

A. Ladieu
Yankee Atomic Electric Company
1671 Worcester Road
Framingham, MA 01701

D. S. Rowe
Rowe and Associates
Suite 200
2050 112th Avenue NE
Bellevue, WA 98007

No. of
Copies

Y. Hsii
Division of Systems Integration
Office of Nuclear Regulation
U.S. Nuclear Regulatory
Commission
Washington, DC 20555

L. Phillips
Division of Systems Integration
Office of Nuclear Regulation
U.S. Nuclear Regulatory
Commission
Washington, DC 20555

L. Agee
Electric Power Research
Institute
P.O. Box 10412
Palo Alto, CA 94303

R. Lambert
Electric Power Research
Institute
P.O. Box 10412
Palo Alto, CA 94303

G. S. Srikantiah
Electric Power Research
Institute
P.O. Box 10412
Palo Alto, CA 94303

R. Rice
EG&G Idaho, Inc.
P.O. Box 1625
Idaho Falls, ID 83415

C. R. Bolmgren
Westinghouse Electric Corp.
Nuclear Waste Department
P.O. Box 3912
Pittsburgh, PA 15230

D. Klein
Mechanical Engineering
Department
University of Texas
Austin, TX 78712

No. of Copies

ONSITE

DOE Richland Operations Office

E. C. Norman/D. E. Kenyon

3 Westinghouse Hanford Company

C. L. Brown
G. T. Harper
R. E. Stover

44 Pacific Northwest Laboratory

G. H. Beeman
D. J. Bradley
J. L. Braitman
J. M. Cuta
J. M. Creer (5)
L. R. Dodd
R. E. Einziger
M. D. Freshley
C. M. Heeb
A. B. Johnson, Jr.
B. M. Johnson
L. T. Lakey
D. L. Lessor
N. J. Lombardo
P. S. Lowery
R. A. McCann (10)
M. A. McKinnon (5)
T. E. Michener
D. R. Rector
C. W. Stewart
D. S. Trent
Technical Report Files (5)
Publishing Coordination (1)